# Active and passive acoustic behavior of bubble clouds at the ocean's surface

A. Prosperetti, N. Q. Lu,[a] and H. S. Kim[b]
*Department of Mechanical Engineering, The Johns Hopkins University, Baltimore, Maryland 21218*

(Received 16 August 1991; revised 11 January 1993; accepted 22 February 1993)

The emission and scattering of sound from bubble clouds is studied theoretically. It is shown that clouds having a size and air content similar to what might be expected as a consequence of the breaking of ocean waves can oscillate at frequencies as low as 100 Hz and below. Thus cloud oscillations may furnish an explanation of the substantial amount of low-frequency wind-dependent oceanic ambient noise observed experimentally. Detailed results for the backscattering from bubble clouds—particularly at low grazing angles—are also presented and shown to be largely compatible with oceanic data. Although the cloud model used here is idealized (a uniform hemispherical cloud under a plane water free-surface), it is shown that the results are relatively robust in terms of bubble size, distribution, and total air content. A similar insensitivity to cloud shape is found in a companion paper [Sarkar and Prosperetti, J. Acoust. Soc. Am. **93**, 3128–3138 (1993)].

PACS numbers: 43.30.Nb, 43.30.Ft, 43.30.Lz

## INTRODUCTION

Recent research has brought to the fore the importance of bubble clouds at the ocean's surface for the propagation and generation of underwater sound (Carey and Bradley, 1985; Carey and Browning, 1988; Prosperetti, 1985, 1988a,b; Lu *et al.*, 1990; Yoon *et al.*, 1991; Lu and Prosperetti, 1993). On the one hand, it has been realized that the clouds can oscillate in collective modes and give rise to acoustic emissions as low as a few tens of Hz irrespective of the size of the constituent bubbles. It is possible that in this fact an explanation may be found of the low-frequency component of wind-dependent oceanic ambient noise that has long puzzled investigators (Wenz, 1962; Kerman, 1984; Carey and Wagstaff, 1986; Kewley *et al.*, 1990). Secondly, several analyses have shown that the backscattering produced by bubble clouds can be quite substantial and preliminary estimates indicate that these entities may be responsible for the unexpectedly high backscattering strengths found experimentally.

The presence of bubbles in substantial numbers in the uppermost several meters of the ocean surface is so well known that a few references will be sufficient in this respect (Monahan, 1971; Thorpe, 1982; Farmer and Vagle, 1989). One may distinguish between the regions of "fresh" bubbles, newly formed by breaking waves, and the "old" bubbles, that are stabilized by still unclear mechanisms and survive long after their formation. Typically, "fresh" bubbles are relatively highly concentrated in clouds very close to the surface, while "old" bubbles are much less dense and are transported downward by turbulence and Langmuir circulation. We refer to these latter agglomeration as bubble "plumes" reserving the term "cloud" for the former.

In this paper we consider both the active and passive facets of the acoustic behavior of bubble clouds. Our model is geometrically simple and consists of hemispherical clouds at the surface of a plane ocean. However, we use a relatively complete model for the bubbly region that goes beyond previous calculations and we solve exactly—rather than in an approximate fashion—the emission and scattering problems. In our basic model the bubble cloud has a uniform spatial distribution of gas and bubble radii. Later, we consider generalizations of this model and try to derive conclusions of more general validity. The dependence of the results on the cloud shape is clearly also important, and is addressed in a separate publication (Sarkar and Prosperetti, 1993a).

Crowther (1980), McDaniel and Gorman (1982, 1983), and McDaniel (1987) have applied incoherent scattering methods to the calculation of backscattering from bubble layers. More recently, McDonald (1991) and Henyey (1991) have treated the backscattering from bubble plumes by the Born approximation. The methods used by these authors are not suitable for the denser bubble assemblies studied in this paper. A detailed comparison of these approaches can be found in Sarkar and Prosperetti (1993a, 1993b).

Perhaps the major piece of information missing for a quantitative description of bubble clouds is the gas concentration by volume, also called void fraction in the multiphase flow literature. Some estimates of this quantity during the active breaking process are as high as 30% (Longuet-Higgins and Turner, 1974; Melville *et al.*, 1992), but this situation of extremely large void fraction must be

[a]Present address: Applied Physics Laboratory, Submarine Technology Department, Hydrodynamics Group, Johns Hopkins Road, Laurel, MD 20723-6099.
[b]Present address: Acoustics Laboratory, Korea Research Institute of Ships and Ocean Engineering, Daeduk Science Town, P.O. Box 1, Daejeon 305-606, Korea.

 0001-4966/93/063117-11$06.00  

very short lived. The gas content under the regions of the surface usually referred to as whitecaps must be much smaller and we use the figure of 1% as a representative order of magnitude. The effect of this variable on the results will also be considered here. Bubble concentration in bubble plumes, on the other hand, is several orders of magnitude smaller (Thorpe, 1982).

## I. MATHEMATICAL MODEL

The mathematical model that we use has already been described in several papers (e.g., Commander and Prosperetti, 1989; Lu *et al.*, 1990; Yoon *et al.*, 1991; Lu and Prosperetti, 1993) and we do not present details here. Suffice it to say that the bubbly liquid is described by means of a Helmholtz equation for an effective medium having a wave number $\kappa$ given by

$$\kappa^2 = k^2 + \frac{4\pi\omega^2 an}{\omega_0^2 - \omega^2 + 2ib\omega}. \tag{1}$$

Here, $k=\omega/c$ is the wave number in the pure liquid, $c$ the speed of sound in the pure liquid, $a$ the equilibrium bubble radius, $n$ the bubble number density, $b$ the frequency-dependent damping "constant," and $\omega_0$ the natural frequency. The explicit expressions for these quantities are somewhat involved and can be found in the above-cited references. Equation (1) is for the case of equal-sized bubbles. The extension to a nonuniform size distribution is straightforward and can be found, e.g., in Commander and Prosperetti (1989) and Lu and Prosperetti (1993).

Two recent papers (Omta, 1987; D'Agostino and Brennen, 1989) present a treatment of the oscillations of a spherical bubble cloud in an unbounded liquid including effects—such as the "slip" velocity of the gas relative to the liquid—that are not present in the theory leading to (1). On a practical level, such effects may be disregarded here as their inclusion leads to indistinguishable results for linear problems and low gas concentrations (see, e.g., Caflisch *et al.*, 1985; Commander and Prosperetti, 1989). It is of conceptual importance, however, that the model used to derive (1) is the only one so far available whose validity to first order in the gas concentration has been proven rigorously by ensemble averaging without *ad hoc* assumptions (Caflisch *et al.*, 1985). Hence, Eq. (1) contains all the terms and the physical effects that survive consistently to first order in the gas volume fraction $\beta$ defined—for equal-size bubbles—by

$$\beta = \tfrac{4}{3}\pi a^3 n. \tag{2}$$

At frequencies much smaller than the resonance frequency of the bubbles and for gas volume fractions larger than about $10^{-4}$, it is easy to show that (1) reduces to the following well-known result for the effective speed of propagation $c_m$ of pressure waves in a bubbly liquid (Wood, 1932; van Wijngaarden, 1972)

$$c_m^2 = P_0/\rho\beta, \tag{3}$$

where $P_0$ is the undisturbed pressure in the liquid and $\rho$ the liquid density. It should be noted that this approximate expression is also valid for general bubble size distributions at frequencies smaller than the resonance frequency of the largest bubbles in the distribution.

The pressure perturbation in the pure liquid is described by the Helmholtz equation with wave number $k$. The transition region between bubbly and clear liquid is modeled as a geometric surface across which the pressure and its normal derivative are continuous.

This model is relatively simple and straightforward. Nevertheless it has been shown to agree remarkably well with experiment both in predicting the velocity of pressure waves and the normal modes of cylindrical bubble clouds (Commander and Prosperetti, 1989; Lu *et al.*, 1990; Yoon *et al.*, 1991; Nicholas *et al.*, 1993).

In the following we shall denote the cloud radius by $R_c$ and we shall use a polar coordinate system $(r,\theta,\phi)$ centered at the cloud's center, with the polar axis directed vertically upward. The time dependence of the disturbances is assumed proportional to $\exp(i\omega t)$. The ocean surface is taken to be plane and pressure release so that on it the perturbation field must satisfy

$$p(r,\theta=\pi/2,\phi)=0. \tag{4}$$

The planarity of the surface is clearly a restriction of the model. For the emission problem, the ocean's roughness will cause a spatial dependence of the intensity different from the idealized one computed below but is not expected to alter our major conclusion, namely that the clouds are capable of oscillation at low frequencies. For the backscattering problem, surface roughness is expected to increase—in a time-average sense—the effect of bubble clouds so that our results should give a lower bound for the backscattering strength. We shall show that, in general, the backscattering strengths that we estimate are in line with the data, while calculations based on surface roughness fall far below (McDaniel and Gorman, 1982). This suggests that surface roughness gives a relatively weak contribution so that its neglect is not entirely unjustified as a first approximation.

## II. BUBBLE CLOUDS AS ACOUSTIC SOURCES

To study the active acoustic behavior of a cloud, in the pure liquid we seek solutions of the Helmholtz equation in the form of outgoing spherical waves,

$$p = h_l^{(2)}(kr)\,Y_{lm}(\theta,\phi), \tag{5}$$

where the amplitude has been set to 1 for convenience, $h^{(2)}$ is a spherical Bessel function of the third kind, and $Y_{lm}$ a spherical harmonic defined by

$$Y_{lm}(\theta,\phi) = \left(\frac{2l+1}{4\pi}\right)^{1/2}\left(\frac{(l-|m|)!}{(l+|m|)!}\right)^{1/2} \times P_l^{|m|}(\cos\theta)\exp(im\phi). \tag{6}$$

These functions are normalized so that

$$\int \bar{Y}_{kl} Y_{mn}\, d\Omega = \delta_{km}\delta_{ln}, \tag{7}$$

where the overbar denotes the complex conjugate, $d\Omega=\sin\theta\, d\theta\, d\phi$ is the element of solid angle, and the integration is extended over the entire solid angle $0\leqslant\theta\leqslant\pi$, $0\leqslant\phi\leqslant 2\pi$.

The pressure-release boundary condition (4) is satisfied by requiring $l+m$ to be an odd integer. Inside the cloud the condition that the pressure perturbation be bounded at $r=0$ requires that it have the form

$$p=A_{lm}\, j_l(\kappa r)\, Y_{lm}(\theta,\phi), \tag{8}$$

where $A_{lm}$ is the amplitude and $j_l$ is a spherical Bessel function of the first kind.

Equating the pressure amplitudes (5) and (8) on the two sides of the surface $r=R_c$ gives

$$A_{lm}=\frac{h_l^{(2)}(kR_c)}{j_l(\kappa R_c)}. \tag{9}$$

With this result, the matching of the normal derivatives gives the following characteristic equation:

$$\frac{uj_l'(u)}{j_l(u)}=\frac{vh_l^{(2)'}(v)}{h_l^{(2)}(v)}, \tag{10}$$

where

$$u=\kappa R_c, \quad v=kR_c. \tag{11}$$

The eigenfrequencies are evidently independent of the order $m$ of the spherical harmonic provided, of course, that $l+m$ is an odd integer. For every $l=1,2,\ldots$ there is an infinity of different modes. Numerical results obtained from this equation are presented in Sec. VI.

## III. ACOUSTIC SCATTERING FROM BUBBLE CLOUDS

We now consider the scattering of an incident plane wave. The mathematical technique is very standard and can be found, e.g., in Morse and Feshbach (1953, Chap. 11).

The plane of incidence is taken as the $(x,z)$ plane and the incident wave is written as

$$p_i=\exp[-i(\mathbf{k}\cdot\mathbf{x})]\equiv\exp[-ik(x\sin\alpha_i+z\cos\alpha_i)], \tag{12}$$

where $\alpha_i$ is the angle of incidence, i.e., the angle that the normal to the wave front makes with the $z$ axis.

We write the total pressure field as

$$p=p_i-\exp(-i\mathbf{k}_r\cdot\mathbf{x})+p_s, \tag{13}$$

where $\mathbf{k}_r=(k\sin\alpha_i,-k\cos\alpha_i)$ is the wave number of the wave specularly reflected by the free surface in the absence of the cloud, the effect of which is represented by the third term. Clearly $p_s$ must vanish on the plane $\theta=\pi/2$ so as to satisfy (4). We therefore write

$$p_s=\sum_{l=1}^{\infty}\sum_{\substack{m=-l\\ m+l=\text{odd}}}^{l} B_{lm}h_l^{(2)}(kr)\, Y_{lm}(\theta,\phi). \tag{14}$$

The disturbance pressure field inside the cloud is written as before as a superposition of terms of the form (8). The constants $A_{lm}$ and $B_{lm}$ are determined by the interface conditions. Continuity of the pressure field at $r=R_c$ gives

$$A_{lm}\, j_l(\kappa R_c)-B_{lm}h_l^{(2)}(kR_c)=8\pi(-i)^l j_l(kR_c)\,\bar{Y}_{lm}(\alpha_i,0), \tag{15}$$

while continuity of the normal derivative leads to

$$(\kappa/k)A_{lm}\, j_l'(kR_c)-B_{lm}h_l^{(2)'}(kR_c)=8\pi(-i)^l j_l'(kR_c)\,\bar{Y}_{lm}(\alpha_i,0). \tag{16}$$

In deriving these equations use has been made of the following relation that is readily proved from known properties of the Bessel functions and spherical harmonics:

$$\exp(-i\mathbf{k}\cdot\mathbf{x})-\exp(-i\mathbf{k}_r\cdot\mathbf{x})=8\pi\sum_{l=0}^{\infty}\sum_{\substack{m=-l\\ m+l=\text{odd}}}^{l}(-1)^l j_l(kr)\,\bar{Y}_{lm}(\alpha_i,0)\,Y_{lm}(\theta,\phi). \tag{17}$$

Solution of the system (15) and (16) gives

$$\begin{aligned} A_{lm}&=8\pi(-i)^l\bar{Y}_{lm}(\alpha_i,0)\,U_l(u,v),\\ B_{lm}&=8\pi(-i)^{l+1}\bar{Y}_{lm}(\alpha_i,0)\,T_l(u,v), \end{aligned} \tag{18}$$

where

$$T_l(u,v)=\frac{\mathcal{T}_l(u)-\mathcal{T}_l(v)}{\mathcal{T}_l(u)-\mathcal{H}_l(v)}\frac{j_l(v)}{h_l^{(2)}(v)}, \tag{19}$$

$$U_l(u,v)=\frac{\mathcal{T}_l(v)-\mathcal{H}_l(v)}{\mathcal{T}_l(u)-\mathcal{H}_l(v)}\frac{j_l(v)}{j_l(u)}, \tag{20}$$

with

$$\mathcal{T}_l(z)=\frac{zj_l'(z)}{j_l(z)}, \quad \mathcal{H}_l(z)=\frac{zh_l^{(2)'}(z)}{h_l^{(2)}(z)}, \tag{21}$$

and $u$, $v$ defined in (11).

We define the dimensionless scattering amplitude $f_*$ of the bubble cloud in the usual way by writing that, as $r\to\infty$, $p_s$ approaches

$$p_s\to(R_c/r)\exp(-ikr)f_*(\theta,\phi). \tag{22}$$

From (14), (18) we then find

$$f_*(\theta,\phi)=\frac{8\pi}{ikR_c}\sum_{l=0}^{\infty}\sum_{\substack{m=-l\\ m+l=\text{odd}}}^{l}T_l(u,v)\times\bar{Y}_{lm}(\alpha_i,0)\,Y_{lm}(\theta,\phi). \tag{23}$$

From its definition (22) it is seen that this quantity represents the amplitude that the scattered wave would have at the cloud's surface, if the asymptotic expression of the scattered field were extrapolated there. The dimensionless differential cross section $\sigma_*$ is related to $f_*$ by

$$\sigma_*(\theta,\phi)=(1/\pi)\,|f_*(\theta,\phi)|^2. \tag{24}$$

This quantity represents the usual scattering cross section normalized by the "footprint" of the cloud on the ocean's surface.

Below the resonance frequency of the bubbles the speed of sound in the bubbly mixture is much smaller than in the pure liquid (Wood, 1932; van Wijngaarden, 1972). In these conditions $v \ll |u|$ and (19) becomes, approximately,

$$T_l \simeq j_l(v)/h_l^{(2)}(v), \tag{25}$$

which is the result that would be obtained by imposing the condition $p=0$ on the surface of the hemisphere $r=R_c$ directly (see, e.g., Morse and Feshbach, 1953, Sec. 11.3; Burke and Twersky, 1964). It will be seen below that the scattering from the cloud approaches this "soft" limit already at relatively low volume fractions.

### A. Backscattering strength

The backscattering strength $\Sigma_B$ is defined by (see, e.g., Urick, 1967; McDonald, 1991)

$$\Sigma_B = r^2 I_s / I_i \, \Delta A, \tag{26}$$

where $I_i$ is the sound intensity of the incident wave, $I_s$ the intensity of the wave scattered in the backward direction, $\Delta A$ the ensonified area, and $r$ the distance between $\Delta A$ and the receiver. The definition presupposes that $\Delta A \ll r^2$. From (22) and (24) we find

$$\Sigma_B = (\pi R_c^2/\Delta A)\sigma_*(\pi-\alpha_i,\pi). \tag{27}$$

If the whitecap density is not unrealistically high, one may neglect multiple-scattering effects (Prosperetti and Sarkar, 1992). In this case the ensonified area may be taken equal to the average area surrounding a cloud, which is obtained by considering a large area of the ocean and dividing by the number of whitecaps on it. With this approximation, the ratio in the right-hand side of (27) can be approximated by the whitecap index $W$, i.e., the fraction of the ocean's surface covered by whitecaps, which is approximately known experimentally. A correlation for this quantity is (Monahan and O'Muircheartaigh, 1980)

$$W = 3.86\times 10^{-6} U^{3.41}, \tag{28}$$

where $U$, expressed in m/s, is the wind speed. For wind speeds of 5, 10, and 15 m/s this relation gives $W=9.33\times10^{-4}$, $9.92\times10^{-3}$, and 0.040, respectively. Carey *et al.* (1993) have presented a review and analysis of whitecap index correlations such as (28). They stress the uncertainty with which the exponent of $U$ is known, with possible values as low as 2.55 or as high as 3.75 or more. Since we are only concerned with crude estimates and trends here, this point is of no great concern for the present purposes.

Rather than the incidence angle $\alpha_i$, in the literature it is customary to use the grazing angle $\eta=\pi/2-\alpha_i$. Furthermore, the backscattering strength is expressed in dB according to the definition

$$S(\eta) \equiv 10\log_{10}\Sigma_B = 10\log_{10}\sigma_*(\pi/2+\eta,\pi) + 10\log_{10} W. \tag{29}$$

## IV. SPATIAL VARIATION OF THE GAS DISTRIBUTION

The previous analysis was carried out under the assumption of a spatially uniform distribution of bubbles in the cloud. This assumption is evidently rather unrealistic and the numerical results to be presented below would be quite uninteresting if they were to strongly depend on it. However, it is possible to show on the basis of a simple model of spatial inhomogeneity that the main qualitative features of our results are expected to be quite robust with respect to the detailed spatial distribution of the bubbles.

We consider nonuniform clouds consisting of $N$ concentric spherical shells $R_j \geqslant r \geqslant R_{j+1}$, $j=1,\ldots,N$, with $R_1=R_c$ and $R_{N+1}=0$. In each shell the bubble distribution is uniform with a gas volume fraction $\beta_j$. In the innermost shell the pressure field is given, as before, by a superposition of terms of the form (8), while in all others the appropriate form is

$$p^{(j)} = \sum_{l=0}^{\infty} \sum_{\substack{m=-l \\ m+l=\text{odd}}}^{l} [A_{lm}^{(j)} j_l(\kappa^{(j)} r) + C_{lm}^{(j)} y_l(\kappa^{(j)} r)]\, Y_{lm}(\theta,\phi). \tag{30}$$

By imposing continuity of pressure and normal derivative of the pressure at the innermost surface of discontinuity $r=R_N$, we have

$$y_l(u_{N-1}) C_{lm}^{(N-1)} - j_l(v_N) A_{lm}^{(N)} = -j_l(u_{N-1}) A_{lm}^{(N-1)}, \tag{31}$$

$$u_{N-1}\, y_l'(u_{N-1}) C_{lm}^{(N-1)} - v_N j_l'(v_N) A_{lm}^{(N)} = -u_{N-1}\, j_l'(u_{N-1}) A_{lm}^{(N-1)}. \tag{32}$$

Upon elimination of $A_{lm}^{(N)}$ we have

$$C_{lm}^{(N-1)} = -\xi_l^{(N-1)} \frac{j_l(u_{N-1})}{y_l(u_{N-1})} A_{lm}^{(N-1)}, \tag{33}$$

where

$$\xi_l^{(N-1)} = \frac{\mathcal{J}_l(u_{N-1}) - \mathcal{J}_l(v_N)}{\mathcal{Y}_l(u_{N-1}) - \mathcal{J}_l(v_N)}, \tag{34}$$

with $\mathcal{Y}_l(z)$ defined similarly to (21) with the Bessel function of the second kind $y_l$ replacing that of the first kind $j_l$.

In the same manner, proceeding backward, we can determine $A_{lm}^{(j)}$ and $C_{lm}^{(j-1)}$ in terms of $A_{lm}^{(j-1)}$ to find for, $j=1,2,3,\ldots,N-1$,

$$C_{lm}^{(j-1)} = -\xi_l^{(j-1)} \frac{j_l(u_{j-1})}{y_l(u_{j-1})} A_{lm}^{(j-1)}, \tag{35}$$

where now

$$\xi_l^{(j-1)}=\frac{\mathscr{T}_l(u_{j-1})-\mathscr{T}_l(v_j)+\xi_l^{(j)}S_l(u_j,v_j)[\mathscr{Y}_l(v_j)-\mathscr{T}_l(u_{j-1})]}{\mathscr{Y}_l(u_{j-1})-\mathscr{T}_l(v_j)+\xi_l^{(j)}S_l(u_j,v_j)[\mathscr{Y}_l(v_j)-\mathscr{T}_l(u_{j-1})]}, \tag{36}$$

$$S_l(u,v)=\frac{j_l(u)y_l(v)}{j_l(v)y_l(u)}. \tag{37}$$

## V. NUMERICAL RESULTS: NORMAL MODES

The eigenfrequencies of oscillation of the bubble clouds are given by Eq. (10). If the roots of this equation were real, it is seen upon comparison with the expression (19) for the $l$th partial scattering amplitude that each normal mode would correspond to a pole in the scattering cross section. The nonzero imaginary part of the roots of (10) prevents this from happening exactly, but since this imaginary part is not very large, a close correspondence between the maxima of the scattering cross section and the eigenfrequencies of the cloud remains. Because of this, the eigenfrequencies can be approximately read off the figures for the scattering amplitudes presented in the next section and, conversely, they furnish close predictions for the location of the maxima of the scattering amplitudes. A similar situation was encountered in the case of plane bubble layers considered in Lu and Prosperetti (1993) and holds, of course, quite generally.

For the case of a spherical bubble cloud in an *infinite* liquid the same characteristic equation (10) holds but, since the condition of zero pressure disturbance on the plane surface (4) is not relevant for this case, the lowest value allowed for the index $l$ is $l=0$. With the neglect of liquid compressibility and dissipation effects, Eq. (10) gives then the following relation for the $l=0$ family of normal modes of the cloud:

$$\omega_n^{(0)}=\omega_0\left[1+\frac{3\beta R_c^2}{\pi^2a^2(n+1/2)^2}\right]^{-1/2}, \tag{38}$$

with $n=0,1,2,\ldots$. This is the same result given in Omta [1987, after correction of a misprint in Eq. (125)] and, to the present $O(\beta)$ accuracy, it also coincides with that of D'Agostino and Brennen (1989). For not too large value of $n$, the second term in the square brackets in (38) is usually much greater than 1, so that we approximately find

$$\omega_n^{(0)}\simeq\frac{\pi}{\sqrt{3\beta}}\left(n+\frac{1}{2}\right)\frac{a}{R_c}\omega_0. \tag{39}$$

Since $R_c^3/a^3\simeq N/\beta$, with $N$ the total number of bubbles in the cloud, the lowest mode $n=0$ is therefore seen to be approximately equal to the natural frequency of the constituent bubbles divided by the cube root of $N$ as deduced from other considerations in Lu *et al.* (1990). With Minnaert's (1933) approximate result $\omega_0\simeq(1/a)\sqrt{3\gamma P_0/\rho}$, where $\gamma$ is the ratio of the gas specific heats, Eq. (39) takes the form of a modified Minnaert formula as noted in Carey and Roy (1993).

The studies of the oscillations of spherical bubble clouds in infinite liquids reported in Omta (1987) and D'Agostino and Brennen (1989) considered only the $l=0$ modes of oscillation of the cloud and the eigenfrequencies were identified indirectly from the maxima of the scattering cross section as indicated at the beginning of this section. Here the boundary condition (4) forces us to consider different values of $l$. Furthermore, we tackle Eq. (10) directly. A numerical method useful for this purpose was outlined in Lu and Prosperetti (1993) and some numerical results for the normal modes have already been presented in Lu *et al.* (1990) in terms of the real and imaginary parts of the roots $\omega$ defined by

$$\omega=2\pi\nu+i\alpha. \tag{40}$$

Figures 1 and 2 show the values of $\nu$ and $\alpha$ for the lowest-frequency normal mode of each of the families of modes corresponding to $l=1,2,3,4,5$. The cloud has a radius of 0.5 m and consists of 1-mm-radius bubbles. The natural frequency of these bubbles in isolation would be 3.24 kHz, and the dramatic effects of the mutual interactions in lowering the natural frequencies of the system are quite striking. At $\beta=10\%$ the lowest mode has a frequency of about 35 Hz and the 5th one of about 95 Hz. Although the theory used here probably is not as accurate at these large $\beta$ values as it is up to a few percent, the basic downward trend is expected to be correct with higher-order corrections in $\beta$ well below $\pm 20\%$.

The effect of the cloud radius for a volume fraction of 1% and 1-mm bubbles is shown in Figs. 3 and 4. There is a very rapid fall-off up to a radius of about 0.2 m, after which the decrease is less rapid although still clear. The effect of the bubble radius for a 0.5-m cloud and 1% volume fraction is shown in Figs. 5 and 6. The very broad maximum in these figures corresponds to the frequency of the normal modes approaching that of the individual bubbles. The effect of this interaction is much more pro-

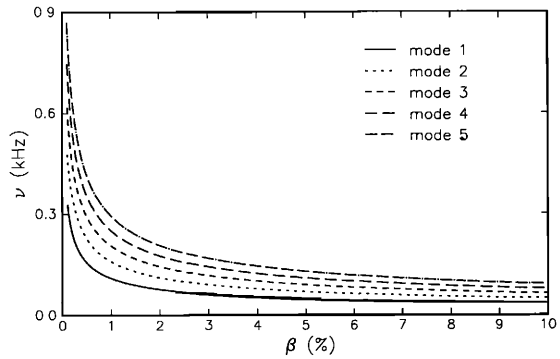


FIG. 1. Real part of the eigenfrequencies (40) of the first normal mode for each of the families $1\leqslant l\leqslant 5$ of a 0.5-m-radius air-bubble cloud as a function of the gas volume fraction $\beta$. The constituent bubbles have a radius of 1 mm with a corresponding natural frequency of 3.24 kHz.

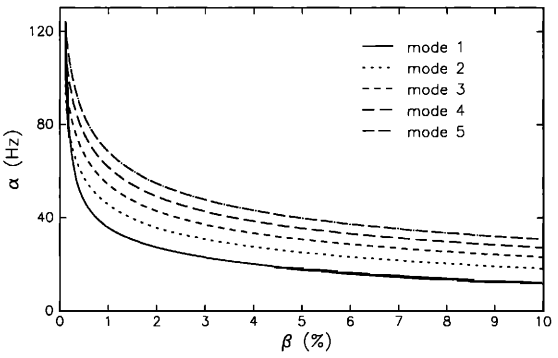


FIG. 2. Imaginary part (damping rate) of the eigenfrequencies (40) of the first normal mode for each of the families $1 \leqslant l \leqslant 5$ of the 0.5-m-radius air-bubble cloud shown in the previous figure as a function of the gas volume fraction.

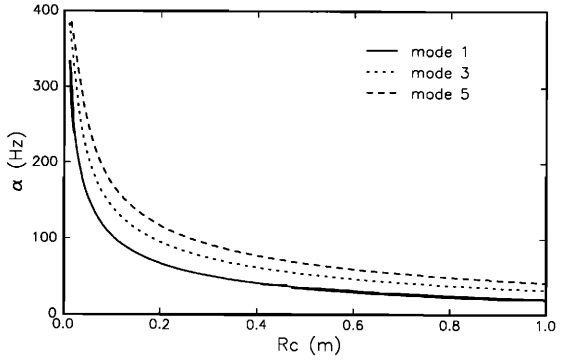


FIG. 4. Imaginary part (damping rate) of the eigenfrequencies (40) of the lowest modes for $l=1$, 3, and 5 of a bubble cloud shown in the previous figure as a function of the cloud's radius.

nounced on the damping of the modes than on the natural frequency, which essentially remains fairly insensitive to the bubble radius.

From Figs. 1, 3, and 5 it can be seen that frequencies of the order of a few hundred Hz can easily be produced over a broad range of volume fractions and cloud and bubble radii. This is precisely the range in which a relatively intense wind-dependent oceanic ambient noise is found (Wenz, 1962; Kerman, 1984; Wille and Geyer, 1984), and the present results therefore strongly support the hypothesis that this component of the noise is due to the free oscillations of bubble clouds (Carey and Bradley, 1985; Carey and Browning, 1988; Prosperetti, 1985, 1988a,b; Lu *et al.*, 1990; Yoon *et al.*, 1991; Lu and Prosperetti, 1993).

As a final point we would like to compare the results obtained by using the correct dispersion relation (1) with those that would follow from use of the simple approximation (3) valid, it may be recalled, far below the resonance of the bubbles. In Fig. 7 we carry out this comparison for the $l=1$, 3, and 5 eigenfrequencies of a cloud with $R_c=0.2$ m comprised of bubbles 2 mm in radius ($\omega_0/2\pi=1.63$ kHz). The two results are very close except when the eigenfrequencies start approaching the resonance frequency of the bubbles. If we look at the damping of the oscillations, however, the picture is quite different as shown in Fig. 8. It is clear here that essentially all of the damping of the cloud's normal modes is provided by the energy dissipation affecting the oscillations of the individual bubbles, rather than by acoustic radiation. Therefore, use of the approximation (3) results in a gross underestimation of the damping at all frequencies.

## VI. NUMERICAL RESULTS: BACKSCATTERING

Typical backscattering data are those obtained by Chapman and Harris (1962; see also Chapman and Scott, 1964) which can be correlated by

$$S(\eta)=3.3b\log(\eta/30)-42.4\log b+2.6, \tag{41}$$

where

$$b=107.5(U\nu^{1/3})^{-0.58}, \tag{42}$$

in which $U$ is again the wind speed in m/s and $\nu=\omega/2\pi$ the frequency. This correlation has been derived on the basis of experiments conducted in the range $0.4\leqslant\nu\leqslant6.4$ kHz, $0\leqslant U\leqslant15.4$ m/s, $3^\circ\leqslant\eta\leqslant40^\circ$, although not the entire ranges were covered for all values of the variables. The scatter of the data around the correlation (41) is given as $\pm3$ dB. In some of our figures we indicate a band with this width. The Chapman–Harris data have been examined on the basis of recent experiments by Ogden and Erskine

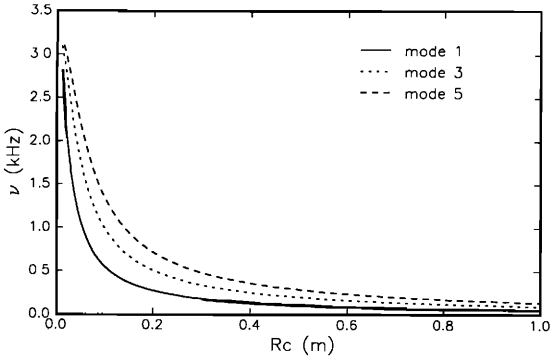


FIG. 3. Real part of the eigenfrequencies (40) of the lowest modes for $l=1$, 3, and 5 of a bubble cloud as a function of the cloud's radius $R_c$. The gas volume fraction is 1% and the radius of the constituent bubbles 1 mm.

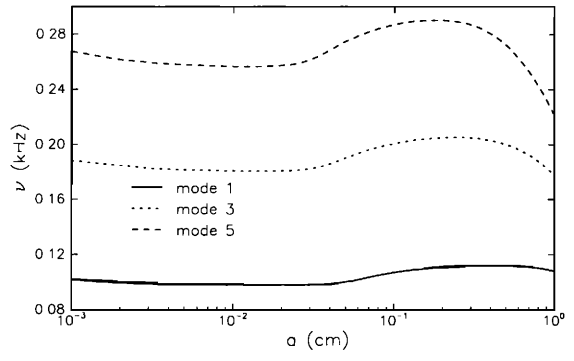


FIG. 5. Real part of the eigenfrequencies (40) of the lowest modes for $l=1$, 3, and 5 of a bubble cloud as a function of the radius $a$ of the constituent bubbles. The gas volume fraction is 1% and the cloud's radius 0.5 m.

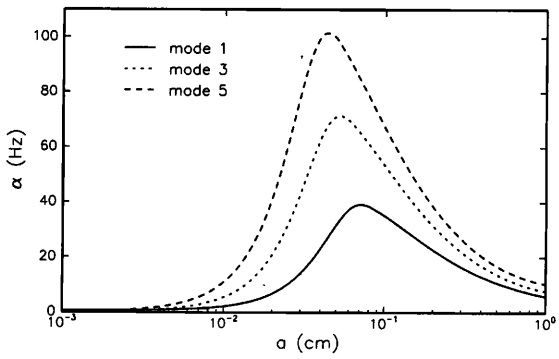


FIG. 6. Imaginary part (damping rate) of the eigenfrequencies (40) of the modes 1, 3, and 5 of a bubble cloud shown in the previous figure as a function of the radius $a$ of the constituent bubbles.

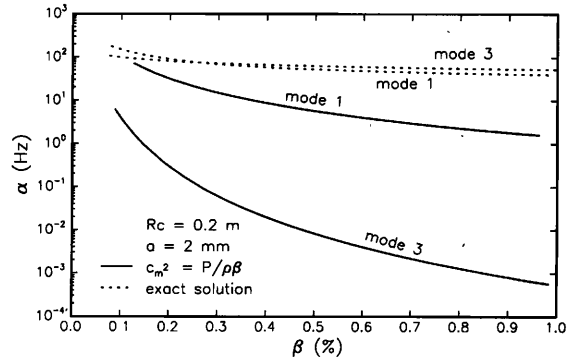


FIG. 8. Comparison between the damping rates of the eigenfrequencies of the lowest modes for $l=1$, 3, and 5 of a 0.2-m-radius bubble cloud as computed with the correct dispersion relation (1) (dashed lines) and the approximate one (3) (solid lines).

(1992) who, at frequencies less than about 200 Hz, find a tendency to over-estimate somewhat the backscattering cross section at wind speeds less than approximately 9 m/s. Since in the numerical examples that follow we are above these values, we can use (41) with some confidence.

In attempting a comparison with our results it must be kept in mind that the theory refers to a single well-defined cloud while the data are averaged over many different clouds of varying size, shape, and volume fraction. Hence the theoretical results have a lot of structure that is not reflected in the data which, in effect, average over many clouds. What is significant, however, is a comparison of the levels and of the general trends of the results.

Typical examples are shown in Figs. 9–11, which refer to grazing angles of 10°, 20°, and 30°, respectively. The left vertical scale gives the dimensionless back-scattering cross section (24), while the right vertical scale indicates the backscattering strength $S$ (29) with $W$ computed for a wind speed $U=10$ m/s. Due to the simple dependence of $S$ upon $W$, from (29), it is seen that the same scale will give the values appropriate to 5, 15, and 20 m/s by subtracting 10.3 dB's or adding 6.00 and 10.3 dB's, respectively. The three lines in these figures refer to clouds with a radius of 0.25 m (dotted lines), 0.5 m (solid lines), and 0.75 m (dash-and-dot lines). In all of them the gas volume fraction is 1% and the undisturbed bubble radius 1 mm (the corresponding natural frequency is $\omega_0/2\pi=3.24$ kHz). The dependence of the results on these parameters will be examined below. Some further backscattering results at large grazing angle, 60° and 90°, are shown in Figs. 12 and 13 for the same three values of the cloud radius.

Comparison with the Chapman–Harris results (hashed bands) reveals a general consistency of the levels and of the trends which suggests the strong possibility that bubble clouds may be responsible for the unexpectedly strong backscattering effect. Although the theoretical results indicate that essentially any desired level may be matched by suitably adjusting the cloud's radius, the comparison that one may make on the basis of these figures is far from empty in that the values assumed to generate these results are reasonable and the experimental trends are closely reproduced. The theoretical levels match the data at 30°, but start falling somewhat below at 20° and much more at 10°. This behavior is consistent with the over-estimation of the Chapman–Harris correlation found by Ogden and Erskine (1992) at frequencies below 200

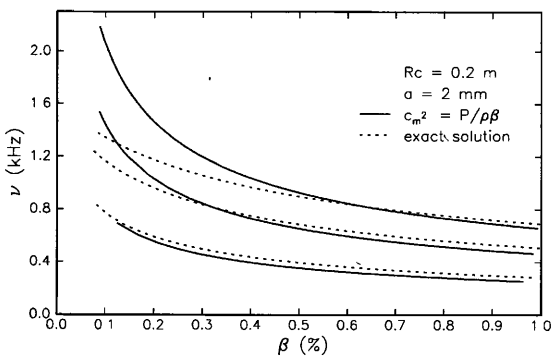


FIG. 7. Comparison between the real part of the eigenfrequencies of the lowest modes for $l=1$, 3, and 5 of a 0.2-m-radius bubble cloud as computed with the correct dispersion relation (1) (dashed lines) and the approximate one (3) (solid lines) as functions of the gas volume fraction. The bubble radius is 2 mm and the corresponding natural frequency 1.63 kHz.

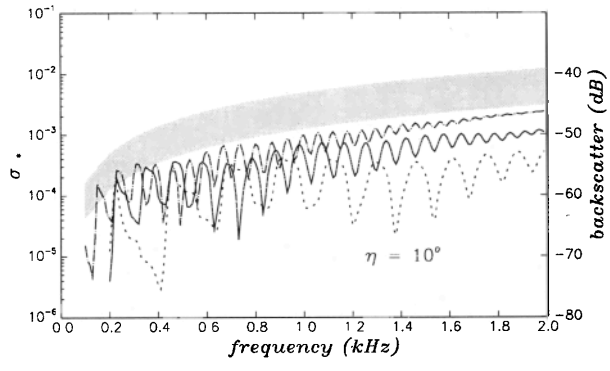


FIG. 9. Dimensionless cross section for backscattering from hemispherical bubble clouds of different sizes (left scale) and backscattering strength for a 10-m/sec wind (right scale) for a 10° grazing angle. The clouds' radii are 0.25 m (dotted line), 0.5 m (solid line), and 0.75 m (dash-and-dot line). The hashed band indicates Chapman and Harris's (1962) data ±3 dB's. The clouds' air volume fraction is 1% and the bubble radius 1 mm.

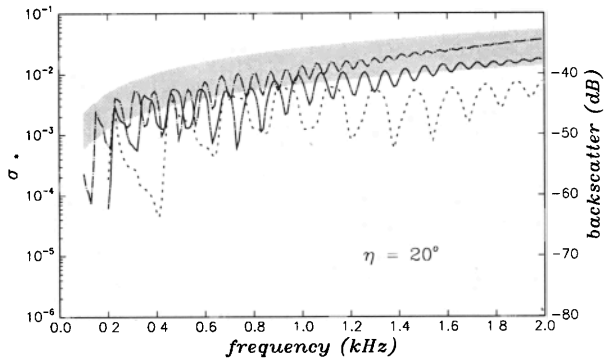


FIG. 10. Dimensionless cross section for backscattering from hemispherical bubble clouds of different sizes (left scale) and backscattering strength for a 10-m/s wind (right scale) for a 20° grazing angle. The clouds' radii are 0.25 m (dotted line), 0.5 m (solid line), and 0.75 m (dash-and-dot line). The hashed band indicates Chapman and Harris's (1962) empirical correlation ±3 dB's. The clouds' air volume fraction is 1% and the bubble radius 1 mm.

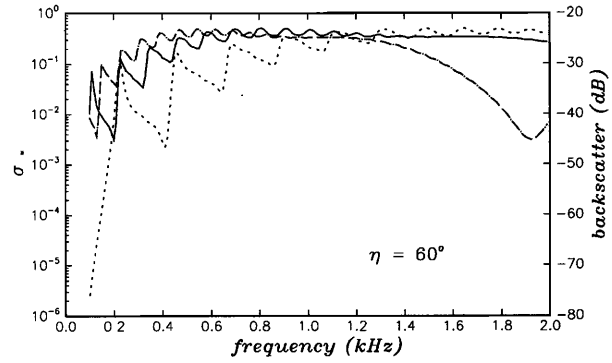


FIG. 12. Dimensionless cross section for backscattering from hemispherical bubble clouds of different sizes (left scale) and backscattering strength for a 10-m/s wind (right scale) for a 60° grazing angle. The clouds' radii are 0.25 m (dotted line), 0.5 m (solid line), and 0.75 m (dash-and-dot line). The clouds' air volume fraction is 1% and the bubble radius 1 mm.

Hz. In addition, the effect of surface roughness becomes increasingly important at very low grazing angles (Dashen *et al.*, 1990). A reviewer has pointed out that the gap between theory and experiment increases somewhat with increasing wind speed contrary to what might be expected on this basis. Other compensating effects may however come into play at higher wind speeds. For example, the depth reached by the bubbles may increase faster than the whitecap surface coverage, giving rise to prolate plumes that are more efficient scatterers (Sarkar and Prosperetti, 1993a). The downward turbulent transport of the bubbles may also increase giving longer residence times for the sub-surface bubbles, which again might not be reflected in the increase with wind speed of the whitecap index. As a matter of fact, the explanation usually accepted for the experimental fact that the intensity of ambient noise decreases at very large wind speeds is the screening effect of a relatively thick layer of bubbles that forms at the ocean surface (Lemon and Farmer, 1984). In this connection see also the final comments of Sec. VII.

Figure 14 shows the dependence of the dimensionless backscattering cross section (left vertical scale) and backscattering strength for 10-m/s winds (right vertical scale) on the grazing angle for a cloud radius of 0.5 m. The dotted line is for a frequency of 0.25 kHz, the dashed line for 0.5 kHz, and the dash-and-dot line for 2 kHz. The three solid lines are the Chapman–Harris correlation (41) for the three frequencies. As can be seen from Figs. 9–11, the corresponding results for 0.2 kHz, for example, would be more than 10 dB's lower than those for 0.25 kHz. This remark illustrates the sensitive dependence of the low-frequency scattering on the detailed conditions, but such dependence would not be observed in the presence of a number of clouds of different size and geometries. This conclusion is motivated by the results of Figs. 9–11 which, qualitatively, can also be interpreted as giving the behavior of the cloud for a fixed frequency and variable cloud radius.

The effect of the gas volume fraction in the cloud is shown in Fig. 15 where the dotted line is for 0.25 kHz, the solid line for 0.5 kHz, and the dashed line for 2 kHz. The

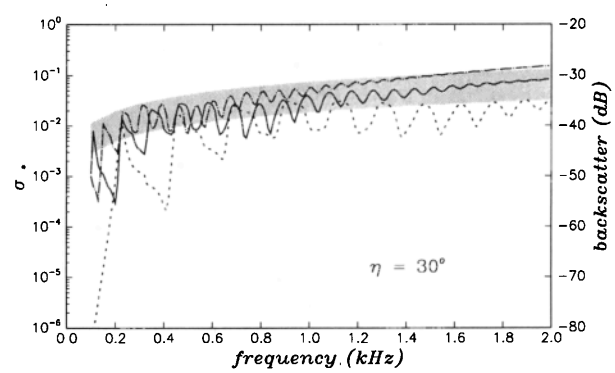


FIG. 11. Dimensionless cross section for backscattering from hemispherical bubble clouds of different sizes (left scale) and backscattering strength for a 10-m/s wind (right scale) for a 30° grazing angle. The clouds' radii are 0.25 m (dotted line), 0.5 m (solid line), and 0.75 m (dash-and-dot line). The hashed band indicates Chapman and Harris's (1962) empirical correlation ±3 dB's. The clouds' air volume fraction is 1% and the bubble radius 1 mm.

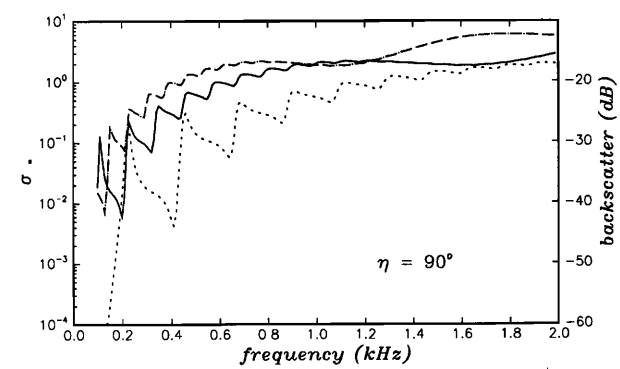


FIG. 13. Dimensionless cross section for backscattering from hemispherical bubble clouds of different sizes (left scale) and backscattering strength for a 10-m/s wind (right scale) for a 90° grazing angle. The clouds' radii are 0.25 m (dotted line), 0.5 m (solid line), and 0.75 m (dash-and-dot line). The clouds' air volume fraction is 1% and the bubble radius 1 mm.

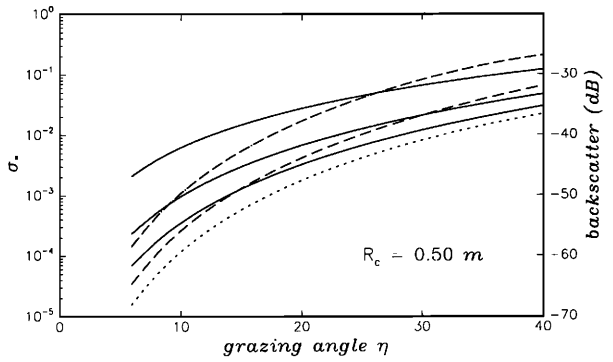


FIG. 14. Dimensionless cross section for backscattering from a 0.5-m-radius hemispherical bubble cloud (left scale) and backscattering strength for a 10-m/s wind (right scale) as a function of the grazing angle at frequencies of 0.25 kHz (dotted line), 0.5 kHz (dashed line), and 2 kHz (dash-and-dot line). The air volume fraction is 1% and the bubbles' radius 1 mm. The three solid lines are Chapman and Harris's (1962) empirical correlation for the three frequencies.

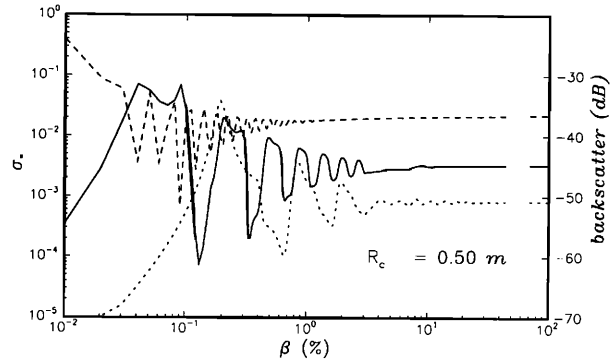


FIG. 15. Dimensionless cross section for backscattering from a 0.5-m-radius hemispherical bubble cloud (left scale) and backscattering strength for a 10-m/s wind (right scale) as a function of the cloud's air volume fraction at frequencies of 0.25 kHz (dotted line), 0.5 kHz (solid line), and 2 kHz (dashed line). The three horizontal segments at the right indicate the result (25) for a completely "soft" cloud. The radius of the bubbles is 1 mm.

short horizontal segments along the right scale indicate the asymptotic result (25) for "soft" hemispheres. This figure clearly demonstrates an effect of "saturation," which occurs earlier and earlier as the frequency is increased. At 2 kHz the scattering is essentially the same as from a completely pressure-release boundary already at a gas volume fraction of the order of a few parts per thousand. At 0.5 kHz this statement starts applying around 1%, and at 0.25 kHz at a few percent.

### A. Spatial heterogeneity

The robustness of the theoretical predictions illustrated previously can be better appreciated by the consideration of a few examples in which the cloud consists of concentric shells with different bubble distributions as described in Sec. IV. Since the emphasis in this paper is primarily on low-frequency effects and since, as was shown above, the bubble radius does not play an important role provided that the frequency is below the resonance frequency of the bubbles, we shall keep the bubble radius $a=1$ mm and only vary the number density.

Figure 16 compares, as a function of frequency, the backscattering cross section at 30° grazing angle for a 1-m cloud. The solid line is for a uniform 1% bubble distribution, while the dashed one is for $\beta=0$ for $0\leqslant r\leqslant R_1=0.75$ m, while $\beta=1\%$ in $R_1\leqslant r\leqslant R_c$. Some differences of the order of $\pm 5$ dB's are apparent at lower frequencies, but the results are remarkably close at higher ones. Another comparison of the same nature is shown in Fig. 17, which refers to a much smaller cloud, $R_c=0.2$ m, and in which the backscattering cross section is plotted as a function of the grazing angle for $\nu=0.5$ kHz. Here the top curve is for a 5-cm-thick, 1% volume fraction band, and the underlying curves are, in order, for a "soft" hemisphere, a 5-cm, 20% band, a 5-cm, 5% band, and a uniform 1% bubble distribution. There are of course differences as one goes from a 5-cm-thick layer of bubbly liquid to a uniform distribution and between 1% and 20% gas volume fraction, but the results are, by and large, relatively close to one another. The fact that a 5-cm, 1% band (top curve) gives a higher backscattering than a uniform 1% gas distribution (lowest curve) indicates of course that resonance effects are present here.

A stronger dependence on the detailed gas distribution is however observed at lower volume fractions. An example is given in Figs. 18 and 19 which show the backscattering cross section from a 1-m cloud at a grazing angle of 20° and frequencies of 0.5 and 2 kHz as a function of the average gas volume fraction $\bar{\beta}$ defined by

$$\bar{\beta}=\Sigma \mathscr{V}_i \beta_i / \mathscr{V}_i, \tag{43}$$

where the $\mathscr{V}_i$'s are the volumes of the concentric hemispherical shells into which the cloud is divided. In this case there are two regions enclosing equal volumes and the three curves correspond to $\beta_{\text{inner}}/\beta_{\text{outer}}=1$ (uniform cloud), 2, and 3.

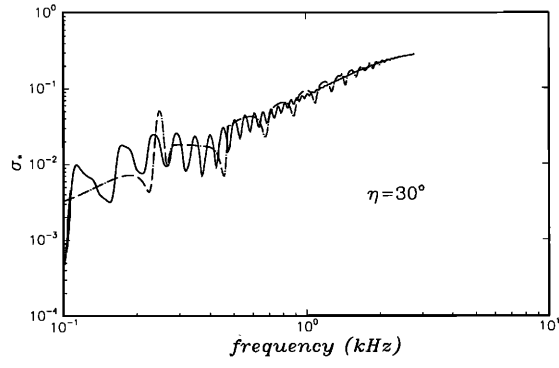


FIG. 16. Dimensionless cross section for backscattering from a 1-m-radius hemispherical bubble cloud as a function of frequency at a grazing angle of 30°. The solid line is for a uniform 1% air volume fraction distribution. The dash-and-dot line is for a 1% air volume fraction distribution in the outer shell 0.75 m $\leqslant r\leqslant$ 1 m, with no bubbles for $0\leqslant r\leqslant 0.75$ m. The radius of the bubbles is 1 mm.

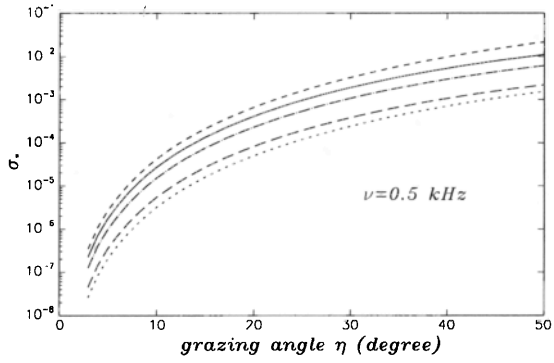


FIG. 17. Dimensionless cross section for backscattering from a 0.2-m-radius hemispherical bubble cloud as a function of the grazing angle for a frequency of 0.5 kHz and different bubble distributions. The top line (medium-dashed) is for a 5-cm-thick, 1%-volume fraction layer of bubbles at the outer edge of the cloud, the second line (solid) is for a completely "soft" cloud, the third line (dash-and-dotted) is for a 5-cm band with a volume fraction of 20%, the fourth line (long-dashed) is for a 5-cm band with a volume fraction of 5%, and the lowest curve (dotted) is for a uniform 1%-air volume fraction distribution. The radius of the bubbles is 1 mm.

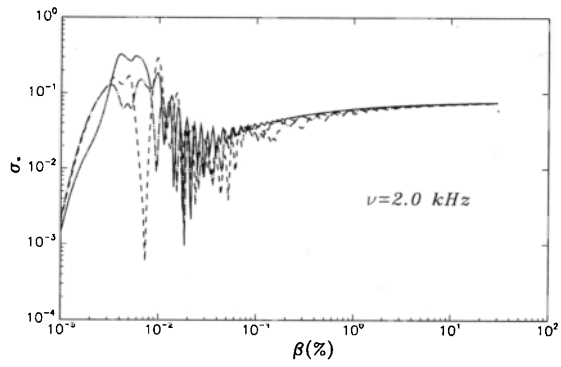


FIG. 19. Effect of the volume fraction distribution on the dimensionless cross section for backscattering from a 1-m-radius hemispherical bubble cloud as a function of the average air volume fraction (43) at 2 kHz and 20° grazing angle. The solid line is for a uniform bubble distribution. For the other two lines the cloud's volume is divided into two equal parts. The dashed line is for the inner region having a volume fraction double that of the outer one, and the dash-and-dotted line for three times as large. The radius of the bubbles is 1 mm.

## VII. CONCLUSIONS

In the present paper we have studied the active and passive acoustic behavior of an idealized model of an oceanic bubble cloud, a half-hemisphere below the surface of a plane ocean. In spite of the simplifications introduced in the model, our results enable us to reach some interesting conclusions. In the first place, we have shown that bubble clouds possess normal modes in the range of a few hundred or even a few tens of Hz. The oscillations of the clouds give then a plausible mechanism for the explanation of the wind-dependent component of oceanic ambient noise at low frequencies. In nature, the excitation of the normal modes is probably due to the same mechanism that produces the bubble clouds in the first place, namely breaking waves. Other mechanisms, such as turbulence, may however exist. As shown in Fig. 8, the damping affecting the cloud emissions is large and arises mainly from the thermal effects associated with the oscillations of the constituent bubbles, rather than from acoustic radiation. Accordingly, the $Q$ of the cloud resonances is not very large.

For the passive case we have studied in some detail the backscattering problem. Our analysis leads to results that are in general quite compatible with the Chapman–Harris data, which suggests that bubble clouds may be responsible for the anomalously high levels observed by these and other investigators. We have shown that, as soon as the cloud's volume fraction of air reaches a few percent, the scattering results are nearly indistinguishable from a completely acoustically "soft" cloud. This finding suggests a scattering mechanism that, in very crude terms, may be described as follows. The scattering occurs not at the ocean's surface, but at some surface below the air-water separation which marks a transition between a region with "few" or no bubbles to one with "many" bubbles. This "effective" scattering surface can evidently be far more irregular than the ocean's surface since its slope is not limited by wave stability, breaking, etc. Correspondingly, the scattering is very much stronger. Clearly, a considerable amount of work—mostly experimental—is needed to put this picture on a firmer quantitative ground.

In a companion paper (Sarkar and Prosperetti, 1993a), the present results are extended to bubble clouds of several different shapes. The conclusions of that study are perfectly compatible with the present ones and prove the "robustness" of the results with respect to changes in the details of the model.

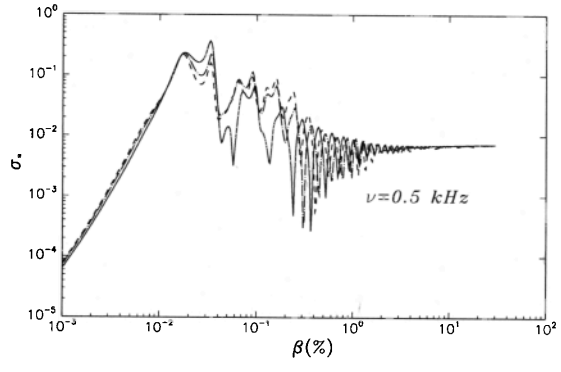


FIG. 18. Effect of the volume fraction distribution on the dimensionless cross section for backscattering from a 1-m-radius hemispherical bubble cloud as a function of the average air volume fraction (43) at 0.5 kHz and 20° grazing angle. The solid line is for a uniform bubble distribution. For the other two lines the cloud's volume is divided into two equal parts. The dashed line is for the inner region having a volume fraction double that of the outer one, and the dash-and-dotted line for three times as large. The radius of the bubbles is 1 mm.

## ACKNOWLEDGMENTS

We would like to thank Dr. A. M. Lezzi for his contribution to the analysis in the early stages of this work and K. Sarkar for some help with the final computations. The reviewers have provided some valuable suggestions. This study has been supported by the Ocean Acoustics Program of the Office of Naval Research.

Burke, J. E., and Twersky, V. (**1964**). "On scattering of waves by an elliptic cylinder and by a semielliptic protuberance in a grounded plane," J. Opt. Soc. Am. **54**, 732–744.
Caflisch, R. E., Miksis, M. J., Papanicolaou, G. C., and Ting, L. (**1985**). "Effective equations for wave propagation in bubbly liquids," J. Fluid Mech. **153**, 259–273.
Carey, W. M. and Bradley, M. P. (**1985**). "Low-frequency ocean surface noise sources," J. Acoust. Soc. Am. Suppl. 1 **78**, S1–S2.
Carey, W. M., and Browning, D. (**1988**). "Low-frequency ocean ambient noise: Measurement and theory," in *Sea Surface Sound*, edited by B. R. Kerman (Kluwer, Boston), pp. 361–376.
Carey, W. M., Fitzgerald, J. W., and Browning, D. G. (**1993**). "Low frequency noise from breaking waves," in *Natural Physical Sources of Underwater Sound*, edited by B. R. Kerman (Reidel, Dordrecht) (to appear).
Carey, W. M., and Roy, R. A. (**1993**). "Sound scattering from microbubble distributions near the sea surface," in *Proceedings of the SACLANT Reverberation Symposium* (Kluwer, Boston) (to appear).
Carey, W. M., and Wagstaff, R. A. (**1986**). "Low-frequency noise fields," J. Acoust. Soc. Am. **80**, 1523–1526.
Chapman, R. P., and Harris, J. (**1962**). "Surface backscattering strengths measured with explosive sound sources," J. Acoust. Soc. Am. **34**, 1592–1597.
Chapman, R. P., and Scott, H. D. (**1964**). "Surface backscattering strengths measured over an extended range of frequencies and grazing angles," J. Acoust. Soc. Am. **36**, 1735–1737.
Commander, K. W., and Prosperetti, A. (**1989**). "Linear pressure waves in bubbly liquids: Comparison between theory and experiment," J. Acoust. Soc. Am. **85**, 732–746.
Crowther, P. A. (**1980**). "Acoustic scattering from near-surface bubble layers," in *Cavitation and Inhomogeneities in Underwater Acoustics*, edited by W. Lauterborn (Springer, New York), pp. 194–204.
D'Agostino, L., and Brennen, C. E. (**1989**). "Linearized dynamics of spherical bubble clouds," J. Fluid Mech. **199**, 155–176.
Dashen, R., Henyey, F. S., and Wurmser, D. (**1990**). "Calculations of acoustic scattering from the ocean surface," J. Acoust. Soc. Am. **88**, 310–323.
Farmer, D. M., and Vagle, S. (**1989**). "Waveguide propagation of ambient sound in the ocean-surface bubble layer," J. Acoust. Soc. Am. **86**, 1897–1908.
Henyey, F. S. (**1991**). "Acoustic scattering from oceanic microbubble plumes in the 100 Hz to 2 kHz region," J. Acoust. Soc. Am. **90**, 399–405.
Kerman, B. R. (**1984**). "Underwater sound generation by breaking wind waves," J. Acoust. Soc. Am. **75**, 149–165.
Kewley, D. J., Browning, D. G., and Carey, W. M. (**1990**). "Low-frequency wind-generated ambient noise source levels," J. Acoust. Soc. Am. **88**, 1894–1902.
Lemon, D. D., and Farmer, D. M. (**1984**). "The influence of bubbles on ambient noise in the ocean at high wind speeds," J. Phys. Oceanogr. **14**, 1762–1778.
Longuet-Higgins, M. S., and Turner, J. S. (**1974**). "An 'entraining plume' model of a spilling breaker," J. Fluid Mech. **63**, 1–20.
Lu, N. Q., Prosperetti, A., and Yoon, S. W. (**1990**). "Underwater noise emissions from bubble clouds," IEEE J. Ocean. Eng. **15**, 275–281.
Lu, N. Q., and Prosperetti, A. (**1993**). "Active and passive acoustic behavior of bubbly layers," J. Acoust. Soc. Am. (submitted).
McDaniel, S. T. (**1987**). "Vertical spatial coherence of backscatter from bubbles," IEEE J. Ocean. Eng. **OE-12**, 349–356.
McDaniel, S. T., and Gorman, A. D. (**1982**). "Acoustic and radar sea surface backscatter," J. Geophys. Res. **87**, 4127–4136.
McDaniel, S. T., and Gorman, A. D. (**1983**). "Spectral spread of sea-surface reverberation," J. Acoust. Soc. Am. **74**, 241–248.
McDonald, B. E. (**1991**). "Echoes from vertically striated subresonant bubble clouds: A model for ocean surface reverberation," J. Acoust. Soc. Am. **89**, 617–622.
Melville, W. K., Lamarre, E., and Loewen, M. R. (**1992**), "The dynamics and acoustics of breaking waves," J. Acoust. Soc. Am. **91**, 2322 (A).
Minnaert, M. (**1933**). "On musical air bubbles and the sound of running water," Philos. Mag. **16**, 235–248.
Monahan, E. C. (**1971**). "Oceanic whitecaps," J. Phys. Oceanogr. **1**, 139–144.
Monahan, E. C., and O'Muircheartaigh, I. G. (**1980**). "Optimal power-law description of oceanic whitecap coverage dependence on wind speed," J. Phys. Oceanogr. **10**, 2094–2099.
Morse, P. M., and Feshbach, H. (**1953**). *Methods of Theoretical Physics* (McGraw-Hill, New York).
Nicholas, M., Roy, R. A., Crum, L. A., Oğuz, H. N., and Prosperetti, A. (**1993**). "Sound emissions by a laboratory bubble cloud," J. Acoust. Soc. Am. (submitted).
Ogden, P. M., and Erskine, P. T. (**1992**). "An empirical prediction algorithm for low-frequency acoustic surface scattering strengths," Report NRL/FR/5160-92-9377, Naval Research Laboratory, Washington, DC 20375-5000.
Omta, R. (**1987**). "Oscillations of a cloud of bubbles of small and not so small amplitude," J. Acoust. Soc. Am. **82**, 1018–1033.
Prosperetti, A. (**1985**). "Bubble-related ambient noise in the ocean," J. Acoust. Soc. Am. Suppl. 1 **78**, S2.
Prosperetti, A. (**1988a**). "Bubble dynamics in oceanic ambient noise," in *Sea Surface Sound*, edited by B. R. Kerman (Kluwer, Boston), pp. 151–171.
Prosperetti, A. (**1988b**). "Bubble-related ambient noise in the ocean," J. Acoust. Soc. Am. **84**, 1042–1054.
Prosperetti, A., and Sarkar, K. (**1992**). "Enhanced backscattering from bubble cloud distributions on the ocean surface," J. Acoust. Soc. Am. **91**, 2315(A).
Sarkar, K., and Prosperetti, A. (**1993a**). "Backscattering of underwater noise by bubble clouds," J. Acoust. Soc. Am. **93**, 3128–3138 (1993).
Sarkar, K., and Prosperetti, A. (**1993b**). "Coherent and incoherent effects in underwater scattering from bubbles," J. Acoust. Soc. Am. (submitted).
Thorpe, S. A. (**1982**). "On the clouds of bubbles formed by breaking wind-waves in deep water, and their role in air-sea gas transfer," Philos. Trans. R. Soc. London Ser. A **304**, 155–210.
Urick, R. J. (**1967**). *Principles of Underwater Sound for Engineers* (McGraw-Hill, New York), Chap. 8, p. 188.
van Wijngaarden, L. (**1972**). "One-dimensional flow of liquids containing small gas bubbles," Ann. Rev. Fluid Mech. **4**, 369–396.
Wenz, G. M. (**1962**). "Acoustic ambient noise in the ocean: Spectra and sources," J. Acoust. Soc. Am. **34**, 1936–1956.
Wille, P. C., and Geyer, D. (**1984**). "Measurements on the origin of the wind-dependent ambient noise variability in shallow water," J. Acoust. Soc. Am. **75**, 173–185.
Wood, A. B. (**1932**). *A Textbook of Sound* (Bell, London).
Yoon, S. W., Crum, L. A., Prosperetti, A., and Lu, N. Q. (**1991**). "An investigation of the collective oscillations of a bubble cloud," J. Acoust. Soc. Am. **89**, 700–706.